AAC Journals.ASM.org

Adaptation of *Enterococcus faecalis* to Daptomycin Reveals an Ordered Progression to Resistance

Corwin Miller,[a] Jiayi Kong,[a] Truc T. Tran,[b] Cesar A. Arias,[b,c,d] Gerda Saxer,[a] Yousif Shamoo[a,e]

Department of Biochemistry and Cell Biology, Rice University, Houston, Texas, USA[a]; Department of Internal Medicine, Division of Infectious Disease, Laboratory for Antimicrobial Research, Houston, Texas, USA[b]; Department of Microbiology and Molecular Genetics, University of Texas Medical School at Houston, Houston, Texas, USA[c]; Molecular Genetics and Antimicrobial Resistance Unit, Universidad El Bosque, Bogota, Colombia[d]; Department of Ecology and Evolutionary Biology, Rice University, Houston, Texas, USA[e]

With increasing numbers of hospital-acquired antibiotic resistant infections each year and staggering health care costs, there is a clear need for new antimicrobial agents, as well as novel strategies to extend their clinical efficacy. While genomic studies have provided a wealth of information about the alleles associated with adaptation to antibiotics, they do not provide essential information about the relative importance of genomic changes, their order of appearance, or potential epistatic relationships between adaptive changes. Here we used quantitative experimental evolution of a single polymorphic population in continuous culture with whole-genome sequencing and allelic frequency measurements to study daptomycin (DAP) resistance in the vancomycin-resistant clinical pathogen *Enterococcus faecalis* S613. Importantly, we sustained both planktonic and nonplanktonic (i.e., biofilm) populations in coculture as the concentration of antibiotic was raised, facilitating the development of more ecological complexity than is typically observed in laboratory evolution. Quantitative experimental evolution revealed a clear order and hierarchy of genetic changes leading to resistance, the signaling and metabolic pathways responsible, and the relative importance of these mutations to the evolution of DAP resistance. Despite the relative simplicity of this *ex vivo* approach compared to the ecological complexity of the human body, we showed that experimental evolution allows for rapid identification of clinically relevant adaptive molecular pathways and new targets for drug design in pathogens.

The U.S. Department Health and Human Services has reported that health care-associated infections (HAIs) are the most common complication of a hospital stay and one of the 10 leading causes of death in the United States (1–3). A group of six organisms, collectively known as the "ESKAPE" pathogens, have been singled out by the Infectious Disease Society of America as organisms against which new antibiotics are urgently needed (4). The six "ESKAPE" organisms, i.e., *Enterococcus faecium*, *Staphylococcus aureus*, *Klebsiella pneumoniae*, *Acinetobacter baumannii*, *Pseudomonas aeruginosa*, and *Enterobacter* species, are responsible for the majority of nosocomial infections and frequently "escape" current antibacterial therapy, making them especially challenging to the health care system (5). Vancomycin-resistant enterococci (VRE) are of particular concern due to a lack of reliable bactericidal therapeutic options. As a consequence, the cyclic lipopeptide daptomycin (DAP) is often used "off label" as an antibiotic of last resort for enterococci (6). Unfortunately, cases of resistance to DAP by both *E. faecium* and *Enterococcus faecalis* have already been reported clinically (6–8).

In 2004, the vancomycin-resistant *E. faecalis* (VRE) strain S613 and DAP-resistant variant R712 were isolated from a patient before and after DAP therapy (9). Comparative genomic sequencing identified mutations to three genes associated with resistance: *liaF*, a member of a three-component stress response signaling pathway; *cls*, encoding a cardiolipin (CL) synthase; and *gdpD*, encoding a putative glycerophosphodiesterase (Fig. 1A) (7). Additional genomic studies on DAP resistance in other enterococci also observed mutations in the *liaFSR* stress response pathway, as well as many other genes, whose roles and relative importance remain uncertain (7, 8, 10, 11).

Although whole-genome sequencing (WGS) of clinical strain pairs has done much to elucidate genetic determinants of drug resistance, it cannot identify genes associated with resistance before they are a problem in the clinic. From our previous experience with molecular adaptation (12, 13), we reasoned that a single polymorphic population in a turbidostat could provide a robust and scalable approach to elucidate genes and molecular pathways conferring resistance in clinical pathogens. There is a common expectation that the evolution of antibiotic resistance in a patient is "too complicated" to be recapitulated *in vitro* with any accuracy. While pathogenesis will likely hinge on the complex environment within a patient and interactions between the pathogen and the patient, the biochemical foundations of antibiotic resistance need not. Perhaps surprisingly, we not only accurately identified the alleles known to be associated with daptomycin resistance in enterococci but also uncovered a wealth of new information about the signaling pathways and potential epistatic relationships among the genes associated with resistance. Since quantitative experimental evolution requires only that an organism be culturable, it is particularly useful for organisms such as *E. faecalis* S613 for which molecular genetics is challenging.

Continuous experimental evolution in bioreactors is markedly different from the well-established flask transfer methods that

Received 9 July 2013 Returned for modification 24 July 2013
Accepted 10 August 2013
Published ahead of print 19 August 2013
Address correspondence to Yousif Shamoo, shamoo@rice.edu.
Supplemental material for this article may be found at http://dx.doi.org/10.1128/AAC.01473-13.

doi:10.1128/AAC.01473-13

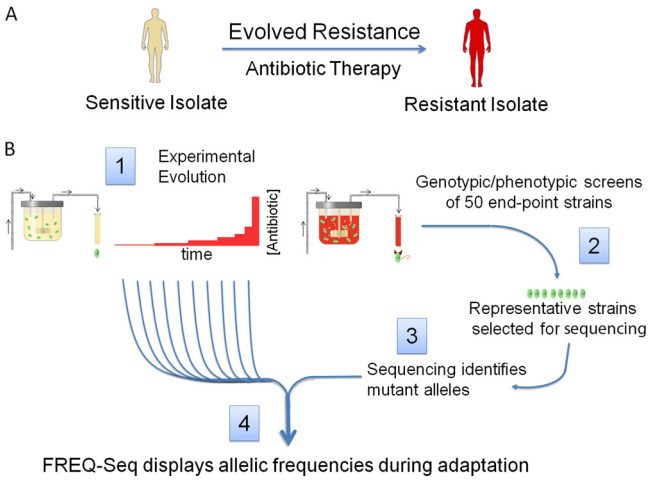

FIG 1 Quantitative experimental evolution and validation against clinically derived strain *E. faecalis* R712. (A) Arias et al. (7) used comparative whole-genomic sequencing of clinical strain pair S613 and R712 to show that mutations to *liaF*, *cls*, and *gdpD* were sufficient to confer DAP resistance. (B) Quantitative experimental evolution combines experimental evolution, genomic sequencing, and measurements of allelic frequencies to identify and deconstruct the adaptive network of genomic changes responsible for resistance. A turbidostat is used for experimental evolution, maintaining a single polymorphic population in exponential growth with the unique capacity to culture both planktonic and biofilm-forming cells (box 1). Phenotypic and genotypic cluster analysis is then used on numerous endpoint strains isolated from the turbidostat (box 2) to identify representative strains for comparative whole-genome sequencing (box 3). Allelic frequencies of mutant genes identified in these strains are then quantified across numerous intermediary populations using the DNA bar-coding technique FREQ-Seq (box 4) (25). Intermediary frequency measurements allow us to identify the most successful alleles and the order of their appearance in the population and to infer their associated mechanisms.

have revolutionized experimental evolution (3, 7, 10, 14–23). Unlike flask transfer experiments, in which populations are subjected to a series of batch cultures and undergo 5 to 10 doublings per day over a range of population sizes and relative drug concentrations, we use a turbidostat to maintain a single large population ($>10^{11}$ total cells) in continuous culture during selection. In our experiments, the turbidostat maintains the population in exponential growth at a constant density, producing over 1,500 generations over 24 days, an important distinction from growth in chemostats (24). Importantly, we maintain both planktonic and nonplanktonic (i.e., biofilm) populations in coculture while we raise the antibiotic concentration. The antibiotic concentration is adjusted each day to the maximal concentration that does not significantly reduce the doubling time of the population. Our objective was to design a method that can apply accurate and controllable selection conditions to a sufficiently large population to rapidly survey accessible adaptive single-nucleotide polymorphisms (SNPs) available to the evolving genome. During a single day (even under nonstressful conditions), we estimate that the entire genome of *E. faecalis* will experience sufficient single-nucleotide mutations to provide a thorough exploration of the genomic sequence space (see Text S1 in the supplemental material). Clonal interference and mutation rate play important roles in adaptation, and under the stress of selection to DAP, it is possible that mutation rates may be significantly higher than basal levels measured for *Escherichia coli* (13, 14).

After adapting cells in the turbidostat, we isolated strains from the evolved population and used genotypic and phenotypic cluster analysis to identify distinct subpopulations. Representative strains were then selected for whole-genome sequencing to build an inventory of mutant alleles. We then measured the frequencies and the order of appearance of the adaptive alleles in the intermediary populations to reconstruct the population dynamics of the successful evolutionary trajectories. Our results demonstrate that despite access to a vast genomic sequence space, adaptive evolution to DAP follows a highly constrained molecular path to resistance.

While we chose adaptation of *E. faecalis* S613 to DAP for this study, we expect that quantitative experimental evolution could be used to rapidly survey, or perform "evolutionary reconnaissance" on, a medically isolated strain that is not easily amenable to many traditional genetic techniques. We envision that quantitative experimental evolution will be used to (i) identify potential pathways of resistance to new antibiotics, (ii) elucidate the intrinsic resistance pathways for other clinical pathogens, and (iii) identify targets for the development of "antievolution" drugs that could be administered to increase the usable life spans of current antibiotics. In its fullest application, quantitative experimental evolution allows us to move from reactive *post hoc* understanding of resistance to a strategy that can anticipate resistance in a predictive manner. By combining the strengths of experimental evolution and genomic analysis of intermediary populations, quantitative experimental evolution provides important insights into drug resistance that are hard to glean from genomic or clinical data alone and can provide a powerful complement to pharmacokinetic and animal studies.

MATERIALS AND METHODS

Summary of methods. The clinically isolated *E. faecalis* strain S613 was continuously cultured in a turbidostat for a total of 31.6 days. Following a 6.7-day-long preadaptation to the laboratory conditions in the absence of drug, cells were exposed to increasing concentration of DAP (up to 20 μg/ml) for 23.8 days. We isolated 50 strains from the final population, confirmed their resistance phenotype by measuring their DAP MIC (MIC_{DAP}) and determined their genotype for *liaF* and *cls*. We selected eight genetically distinct turbidostat-derived DAP-resistant (TDR) clones for whole-genome sequencing (Table 1). The Illumina sequencing reads were aligned to the reference sequence of the ancestral strain S613, and predicted mutations were confirmed by Sanger sequencing. To follow the evolutionary dynamics of the evolved alleles, the whole populations were sequenced at the mutation sites over the course of the experiment, using the DNA bar coding technique FREQ-Seq (25).

Biofilm formation for each TDR strain and population mixture was assayed using overnight growth in microtiter plates, as was the growth rate of each resistant strain. To assess cell morphology and structural changes of *E. faecalis* TDR strains, transmission electron microscopy (TEM) was used as previously described (7). To examine *liaFSR* and *yvlB* operon structures, mRNA was purified from *E. faecalis* S613, converted into cDNA, and used as the template for a series of PCRs.

Bacterial isolates and growth media. *E. faecalis* strains were grown in a broth mixture (LBHI) comprised of 20% brain heart infusion (BHI) and 80% lysogeny broth (LB). Isolation of clinical *E. faecalis* strains S613 and R712 has been described previously (9), as have their whole-genome sequencing and characterization (7).

Turbidostat adaptation to *in vitro* conditions. A Sartorius Stedim Biostat Bplus bioreactor was inoculated from a single colony of *E. faecalis* strain S613 and maintained without DAP to allow cells to equilibrate to turbidostat growth conditions. Cells were grown under steady-state conditions in LBHI medium (250-ml culture volume, 37°C, 50 mg/ml Ca^{2+},

TABLE 1 Functions of DAP resistance-associated alleles[a]

Mutant gene	Protein classification	Putative cellular function
liaF	*liaFSR* signaling pathway regulator	CESR
yvlB	*liaFSR* signaling pathway putative target	CESR
liaR	*liaFSR* signaling pathway regulator	CESR
gshF	Glutathione biosynthesis	Oxidative stress response
yybT	Cyclic dinucleotide phosphodiesterase	Stress signaling
cls	Cardiolipin biosynthesis	Membrane synthesis
drmA	Unknown	Unknown
mdpA	Multidrug resistance pump	Unknown
selA	Selenocysteine biosynthesis	Oxidative stress response

[a] Functions for LiaF, LiaR, YybT, Cls, and SelA are based on homologues in *B. subtilis*. The function of MdpA is based on conserved sequence motifs identified by BLAST, and GshF function is based on its homologue in *Pasteurella multocida*. For linkage of *yvlB* to the *liaFSR* pathway, see Text S1 in the supplemental material. CESR, cell envelope stress response.

TABLE 2 Distinct genotypes of DAP-resistant *E. faecalis* S613 strains derived from a convergent phenotype (DAP resistance)[a]

Strain	Coding change(s) identified during DAP adaptation
TDR4	$liaR^{D191N}$, $cls^{\Delta NFQ74\text{-}76,\ S104L}$, $gshF^{E554K}$, $yybT^{I440S}$
TDR7	$yvlB^{V289fs}$
TDR8	$liaF^{insI177}$, $cls^{\Delta NFQ74\text{-}76}$
TDR13	$liaF^{\Delta I177}$, $cls^{\Delta NFQ74\text{-}76}$, $drmA^{L4stop}$
TDR22	$liaF^{T194I}$, $drmA^{N150fs}$
TDR28	$liaF^{insI177}$, $drmA^{N150fs}$, $mdpA^{F185fs}$
TDR19.1	$yvlB^{V289fs}$, cls^{R218Q}
TDR19.2	$liaR^{D191N}$, $cls^{\Delta NFQ74\text{-}76,\ insAII14\text{-}16}$, $gshF^{E554K}$, $yybT^{I440S}$
R712	$liaF^{\Delta I177}$, $cls^{\Delta K61}$, $gdpD^{\Delta I170}$

[a] Turbidostat-derived (TDR) strains are endpoint isolates from day 23 of experimental evolution. Comparative whole-genome sequencing of the endpoint strains relative to *E. faecalis* S613 revealed adaptive changes associated with adaptation to DAP. All mutations in coding regions are shown (for noncoding changes, see Table S4 in the supplemental material). Δ, deletion; ins, insertion; fs, frameshift.

airflow of 0.16 to 0.2 liter/min). A constant optical density at 600 nm (OD_{600}) of 0.3 ($\sim 3 \times 10^8$ cells/ml) was maintained by automated dilution of the culture from a series of feed reservoirs. Within 12 h following inoculation into the turbidostat, biofilms started to form in the vessel. Once biofilms formed, the total population size could no longer be measured accurately through automation using light scattering, and therefore dilution control parameters were adjusted manually for the entirety of the experiment. A turbidostat-adapted strain of S613 was produced by continuous culture in the turbidostat without antibiotic for 6 days 16.5 h. No endpoint genomic changes were identified following preculturing, suggesting that selection in the LBHI medium under these condition was very weak. Cells from the turbidostat-adapted population were plated on solid LBHI medium, and a single colony was isolated and used to reinoculate the turbidostat. The DAP concentration was raised to 20 μg/ml in seven intervals across approximately 24 days of continuous culture (see Table S1 in the supplemental material). A polymorphic population was maintained by increasing the antibiotic concentration in empirically determined steps during the course of the adaptation. To measure the MIC for the population, we collected a sample of the turbidostat population every day and diluted it 100-fold into test tubes containing 10 ml of fresh LBHI medium and various concentrations of DAP. The growth rate of the sample was determined as a function of DAP concentration in a 10-ml LBHI liquid culture over approximately 12 h. If the growth rate in a test population with elevated drug concentration matched the growth rate at the DAP concentration currently in use, then the DAP concentration in the bioreactor was increased. To ensure that contaminants were not present during continuous culture, samples from the turbidostat were plated each day on both LBHI and bile esculin agar (BEA), and colony morphology was examined. Population samples were collected every 3 to 6 h, supplemented with glycerol, and stored at −80°C. Samples were relatively large (roughly 5×10^9 cells), representing approximately 5% of the total population in the turbidostat. The biofilm was present as particulate material that was continuously sloughed off the vessel surfaces due to the mechanical shear forces produced by rapid stirring and was collected readily.

TDR strain isolation and whole-genome sequencing. Cells from the final day of the turbidostat selection experiment (at a bioreactor DAP concentration of 20 μg/ml) were plated onto solid LBHI medium. Fifty individual colonies were isolated and designated TDR for turbidostat-derived DAP-resistant colony (TDR1 to -18, -19.1, -19.2, and -20 to -48). To identify novel endpoint strains for WGS, we determined the MIC_{DAP} using agar microdilution (26) and sequenced *liaF* and *cls*, two genes previously linked to DAP resistance (7). From the 50 colonies, seven distinct DAP-resistant colonies were selected for WGS (TDR4, -7, -8, -13, -19, -22, and -28). Genomic DNA was isolated using the UltraClean microbial DNA isolation kit (MO BIO, Carlsbad, CA) following the manufacturer's protocols, including an additional lysis step using lysozyme (0.5 mg/ml lysate) and mutanolysin (0.25 μg/ml lysate).

The genomes were sequenced as paired-end reads on an Illumina HiSeq sequencer (SeqWright, Houston, TX). The reads were aligned to the reference sequence of S613 (gff3 file dated 12 November 2010, downloaded from PATRIC at http://www.patricbrc.org) using Seqman NGen by DNAStar Inc as well as BWA and SAMtools (27–29). The average coverage across the seven clones was 496×. Mutation detection was performed using Seqman (DNAStar) and the BWA alignments (based on 90% agreement among reads for SNPs and 50% agreement for indels), and all reported mutations were confirmed using Sanger sequencing.

After closer investigation of the genomic sequencing data, TDR19 turned out to be a mixture of three genetically distinct colonies that were renamed TDR19.1, TDR19.2, and TDR19.3. The last one, TDR19.3, was genetically identical to strain TDR8 and thus is not its own distinct strain. The frequencies of individual mutations in this mixed sample were compared to the results from Sanger sequencing of these loci in multiple individual colonies isolated from the mixed TDR19 frozen stock to get both linkage and frequency information. Mutations identified in each of these eight distinct strains are listed in Table 2.

Intermediary frequency analysis of DAP resistance-linked mutations. Following identification of the DAP resistance-linked mutations shown in Table 2, frequencies of mutant alleles were assessed for every day of the adaptation experiment using FREQ-Seq, a DNA bar code sequencing method described previously (25, 30). Allelic frequencies of 13 mutations identified in Table 2 were measured across 23 days of adaptation (Fig. 2A). Based on our calculated error rate, we decided that we could distinguish true mutations from sequencing errors at a level of 0.5%. Any mutant allele frequencies below 0.5% were treated as missing values.

Biofilm formation assays. Biofilm formation was measured for strains R712, S613, TDR4, TDR7, TDR8, TDR13, TDR19.1, TDR19.2, TDR22, and TDR28 using a crystal violet staining procedure adapted from that described by Mohamed and Huang (31). Turbidostat population mixtures were also assayed at eight time points during turbidostat adaptation (days 2, 4, 3, 18, 20, 22, 23, and 24). The turbidostat population mixtures were plated on BEA using an aliquot of the frozen stock and were propagated on subsequent plates and into liquid broth using loops full of cells to capture the diversity of the evolving population.

Growth rate measurements. Growth rates were measured as a function of DAP concentration using a method previously described by Walkiewicz et al. (30). Growth rates at each DAP concentration were plotted against biofilm formation for each strain, and correlation coefficients were calculated using Microsoft Excel.

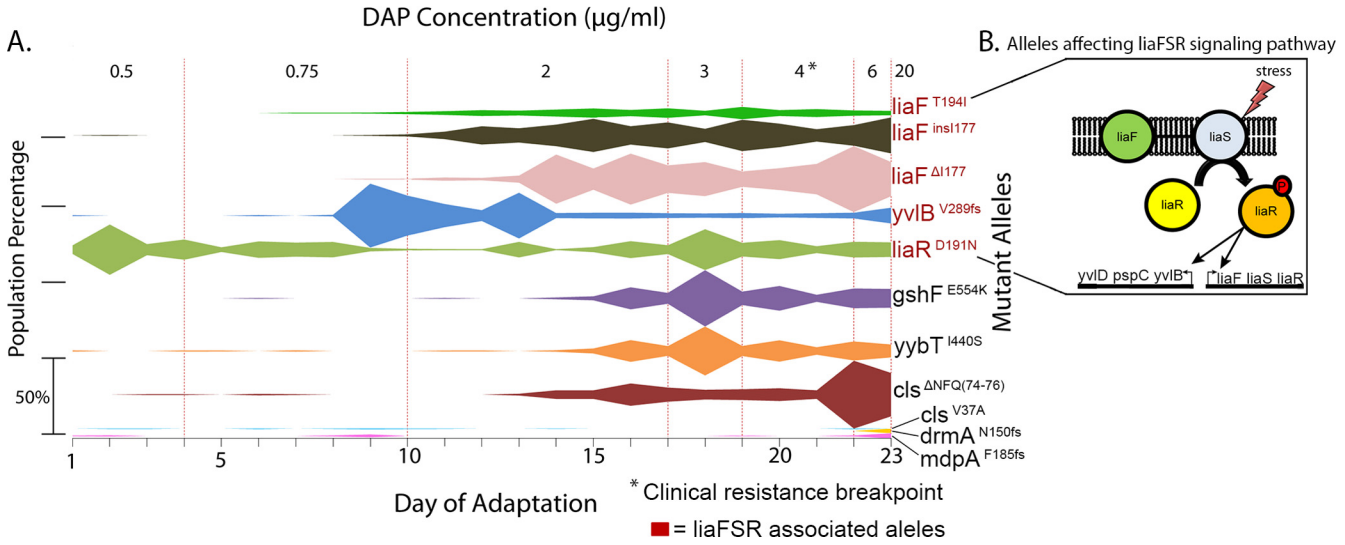

FIG 2 Evolutionary dynamics of 11 alleles associated with DAP resistance during adaptation. (A) The frequencies of the 11 alleles associated with DAP resistance identified from the end of the adaptation (Fig. 1, box 2) were quantitated using the DNA bar-coding technique FREQ-Seq (25) (Fig. 1, box 4) and plotted as a function of time during the experiment (*x* axis). The scale bar on the left indicates a frequency of 50% for a single allele in the population. Note that frequencies correspond to individual alleles, and thus population percentages need not total to 100%. Dotted lines depict changes in DAP concentration, which are labeled on the upper *x* axis. Alleles appearing at a frequency of below 0.5% are not shown. The last frequencies shown are for day 23, but the experiment continued until day 24. *, clinical resistance breakpoint (4 μg/ml DAP). Alleles with names in red affect the three-component LiaFSR signaling system, which is involved in CESR. (B) Proposed functions of *liaFSR* components are based on homologous proteins previously studied in *Streptococcus mutans* (35).

TEM. To assess cell morphology and structural changes of *E. faecalis* TDR strains, transmission electron microscopy (TEM) was used as previously described (7). The thickness of cell walls was measured from the outer border of the cell membrane to the outer edge of the cell wall.

FREQ-Seq analysis of DAP resistance-linked mutations. Following identification of the DAP resistance-linked mutations shown in Table S1 in the supplemental material, frequencies of mutant alleles were assessed for every day of the adaptation experiment using FREQ-Seq, a DNA bar code sequencing method (25, 30). Generation of samples suitable for such deep sequencing required three steps. First, a bar-coded primer was amplified from a plasmid (generously provided by C. Marx, Harvard University) using an Illumina forward primer and an M13 primer. Second, a 100-nucleotide fragment containing a mutation site was amplified with primers containing the same M13 recognition site on the forward primer and the Illumina primer for the reverse reaction on the reverse primer. Finally, a unique bar code was added by amplification of the sample prepared in step 2 with primers generated in step 1, to create an oligonucleotide containing the Illumina primer, a bar-coded sequence, an M13 sequence, and our target sequence.

We used 23 bar codes, one for each day, and sequenced 13 loci per bar code. There was considerable variation in read coverage among days. The read coverage for two bar codes (13 and 21) was too low to give reliable estimates. Therefore, we resequenced those two bar codes and any sample that had a read coverage below 100 reads. The overall average read coverage was 19,321 reads per locus and day (median = 979), with an average coverage of 1,115 reads per locus and day for the first sequencing set (n = 245) and an average coverage of 162,035 for the second set (n = 31).

To assess the frequencies of the different alleles in the populations, we identified all the reads that matched a search query for the wild-type allele (same bases as in the reference sequence S613 at the mutation site) or a mutant allele at the mutation site perfectly. The queries consisted of an A, C, G, or T at the SNP site and the 10 flaking bases up- and downstream. The frequency of a mutant allele was calculated as the number of reads with that particular mutation divided by the total number of alleles with perfect matches (for A, C, G, or T at the SNP site). Indels were approached in a similar way; however, instead of searching for possible SNPs, the search query consisted of the indel sequence and the flanking 10 bases upstream and downstream. To assess the frequencies of mutations, we determined the number of reads with the wild-type sequence, as well as the number of reads with two or one deletion and two or one insertion of the same indel sequence, while the flanking regions of 10 nucleotides upstream and downstream of the mutated region were held constant. The frequency of a mutant allele was calculated as the number of reads with a mutation divided by the total number of reads for this site (which included wild type, two and one insertions, and two and one deletions).

Error rates for single-nucleotide substitutions were also assessed for the four bases (positions) surrounding the SNP (30). The average error rate at a given position was calculated as (1 − frequency of non-wild-type allele)/3, and the average rate for a mutation site was calculated as the average across the four positions surrounding the mutation site. The error rate for a deletion was calculated as [frequency of (2 deletions + 1 insertion + 2 insertions)]/3 and that for an insertion as [frequency of (2 deletions + 1 deletion + 2 insertions)]/3. As *liaF* position 168 had both insertion and deletion mutant alleles, we omitted these two mutations from the error rate calculations. The overall average error rate across sites and days was 0.0018, with a 95% confidence interval (CI) ranging from 0.0016 to 0.002. The average error rate for SNPs was 0.0028 (95% CI, ±0.0002), and that for indels was 0.0003 (±0.00014). Based on this error rate, we decided that we could distinguish true mutations from sequencing errors at a level of 0.5%. Any mutant allele frequencies below 0.5% were treated as missing values.

RNA isolation, cDNA synthesis, and operon mapping. To examine *liaFSR* and *yvlB* operon structures, RNA from *E. faecalis* strain S613 was purified by first growing 10 ml of cells overnight in liquid LBHI culture. Cells were diluted 100-fold and allowed to grow to mid-log phase (OD_{600} = 0.2). Cells were pelleted and enzymatically lysed using lysozyme and mutanolysin (see "TDR strain isolation and whole-genome sequencing" above).

Total RNA was extracted using the RNeasy Mini Kit (Qiagen, Valencia, CA). RNA integrity was confirmed using a denaturing agarose gel. RNA was treated with the DNA-Free Kit (Applied Biosystems, Carlsbad, CA) to remove residual genomic DNA. Removal of DNA was confirmed

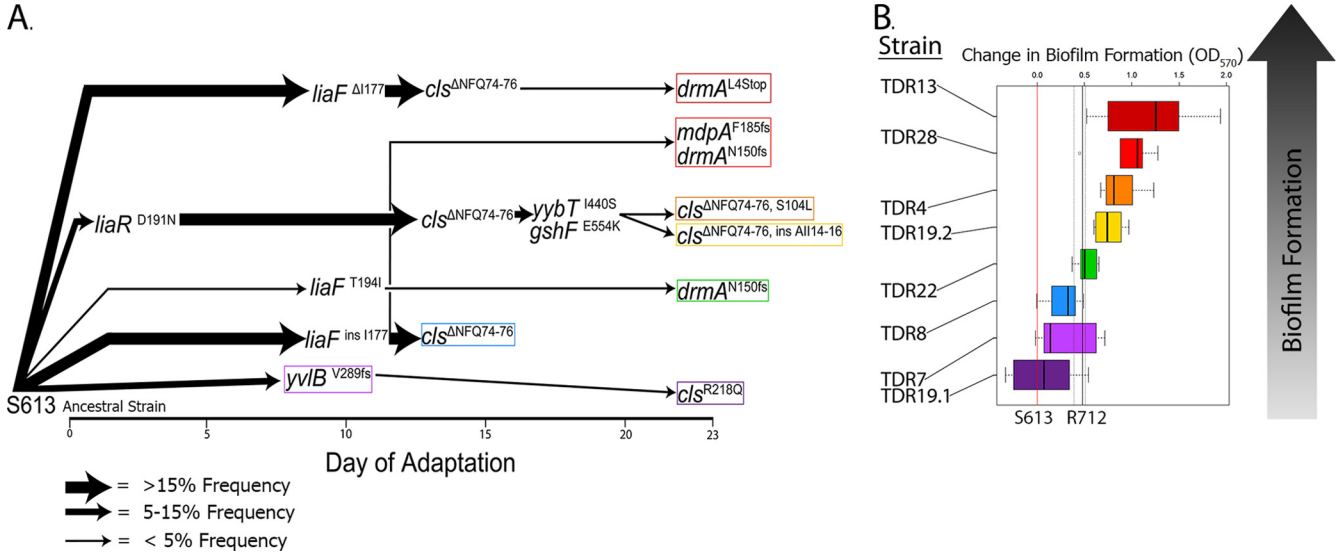

FIG 3 (A) The phylogeny inferred from allelic frequency measurements and linkage in endpoint strains highlights biofilm associated lineages. All the successful evolutionary trajectories involve initial changes directly in the LiaFSR pathway, including a newly identified target operon (*yvlB*). Changes in *cls*, *gshF*, or *yybT*, while potentially important, occur later and are likely epistatic with earlier changes. The line thickness corresponds to the success of a specific genotype by the end of the experiment. Median biofilm formation relative to that of S613 was determined for all the endpoint strains (boxed). (B) Box plots depicts the first and third quartiles of biofilm formation, with the median value shown by a thick black line. The color indicates a specific TDR strain. Error bars extending from each box show the minimum and maximum range of data. Dotted vertical lines show the first and third quartiles of biofilm formation for R712. Biofilm formation was normalized to biofilm formation of S613, shown as a red vertical line.

by the inability to amplify *liaF*, using RNA as the template for a PCR. cDNA was synthesized using the SuperScript III first-strand synthesis kit (Invitrogen Life Technologies, Grand Island, NY).

Strain S613 cDNA was used as the template in a series of PCRs to confirm the structure of the *liaFSR* operon. Using a series of primers, each overlapping two genes, we confirmed that gene 1795 (encoding the putative transcription elongation factor GreA) is not on the same RNA strand as gene 1796 (*liaF*) (see Table S3 in the supplemental material). The three known *liaFSR* components were in turn confirmed to be on the same RNA strand (genes 1796, 1797, and 1798). Finally, gene 1799 (encoding potassium uptake protein TrkA) was found to not be on the same RNA strand as gene 1798 (*liaR*). Using a similar approach, *yvlB* (gene 2118) was confirmed to be on the same RNA strand as gene 2117, a putative *pspC* homologue.

Nucleotide sequence accession number. Genomes of TDR strains are available through NCBI under accession number SRP029594.

RESULTS AND DISCUSSION

Continuous evolution of a single polymorphic population of *E. faecalis* S613 identifies the major evolutionary trajectories to DAP resistance. To identify the important evolutionary trajectories to DAP resistance, we gradually adapted a population of *E. faecalis* S613 to increasing concentrations of DAP in a turbidostat over 24 days (see Table S1 in the supplemental material). At the end of the adaptation, we isolated 50 random endpoint strains from the evolved population and measured the MIC to DAP (MIC_{DAP}) for each strain. All 50 strains had substantially increased MIC_{DAP} values ranging from 2 to 8 μg/ml, compared to values of 0.25 and 4 μg/ml in strains S613 and R712, respectively. These strains were then screened by genotype, using the known clinical resistance markers *liaF*, *cls*, and *gdpD* (7). We identified eight genetically distinct DAP-resistant clusters that represented the most successful evolutionary trajectories within this single population at the end of the experiment. Whole-genome sequencing of a representative strain from each cluster (denoted TDR for turbidostat-derived resistant strain) was then used to compile an inventory of mutant alleles (Table 2).

Among the 50 endpoint strains screened, none had more than one mutation within *liaFSR* (see Table S2 in the supplemental material). The absence of more than one mutant allele in the *liaFSR* pathway within a single evolutionary trajectory suggests that additional mutations to *liaFSR* do not confer substantially more resistance. Furthermore, 48% of the endpoint strains had a mutation to *cls* (see Table S2 in the supplemental material) in the *liaFSR* background. These findings are in good agreement with previous clinical and *in vitro* studies implicating *liaFSR* and *cls* in DAP resistance (7, 8, 10). Mutations in the gene *gdpD* were not observed in any of the 50 strains, which is consistent with other studies indicating that mutations to this gene are rare, highlighting the power of quantitative experimental evolution to successfully identify the most prominent adaptive pathways (7, 8, 10).

The critical first step to DAP resistance is alteration of the LiaFSR cell envelope stress response (CESR) pathway. To deconstruct the adaptive network of genomic changes responsible for DAP resistance, we determined the intermediate allelic frequencies of the mutations identified by whole-genome sequencing using a high-throughput DNA bar code-based method (FREQ-Seq) (25) (Table 2). With this approach, we followed the rise and fall of mutant alleles at frequencies as low as 0.5%, accurately tracking the evolutionary dynamics of the polymorphic population during adaptation (Fig. 2A). By observing when each mutation first appeared in the population, we compared their order of appearance with the endpoint genotype of each TDR strain to infer a phylogeny (Fig. 3A). All successful evolutionary trajectories included an initial mutation to *liaR*, *liaF*, or a newly identified putative down-

stream target of LiaFSR signaling designated *yvlB* due to its homology to *yvlB* in *Bacillus subtilis* (EMBL entry AGA21832) (see Table S3 in the supplemental material).

While allelic frequency measurements showed that mutations within the *liaFSR* pathway appeared first in all the successful evolutionary trajectories and reached the highest overall frequency in the population, we asked how representative they were of the final population. Among the 50 randomly selected endpoint strains, 94% had one of the mutations identified in *liaFSR* or *yvlB*, demonstrating that they are very representative of the overall population. The majority of mutations occurred in *liaF* (78%), with changes in *yvlB* (12%) and *liaR* (4%) comprising the remainder (Table 2). Strikingly, 27% of *liaF* mutants had the same amino acid deletion observed in clinical strain R712 ($liaF^{\Delta I177}$). However, with the exception of $liaR^{D191N}$, none of the aforementioned mutations were prevalent at the early stages of selection (Fig. 2A), suggesting that early adaptation was facilitated through either nongenomic changes, such as transcriptional regulation, or early adaptive genomic changes that had little success later in the population and moved to extinction as the DAP concentration increased. Sequencing of population mixtures isolated from days 3, 10, and 20 did not identify any new adaptive alleles at a minimum frequency of 5% (see Text S1 in the supplemental material). This observation is consistent with the hypothesis that transient responses, such as transcriptional regulation, can convey resistance at low DAP concentrations rather than extinct genotypes. By day 10, the DAP concentration reached 2 μg/ml, which favored the rise of multiple highly successful *liaF* mutants.

LiaFSR is a component of the CESR regulon and responds to changes in cell envelope integrity by regulating downstream genes to counteract damage (32). LiaFSR-mediated responses that lead to remodeling of the cell envelope are consistent with studies suggesting that DAP inserts and subsequently oligomerizes in the membrane in a calcium- and phosphatidylglycerol (PG)-dependent manner, which disrupts the functional integrity of the membrane (33, 34). In *B. subtilis*, LiaF strongly inhibits signaling through LiaS and its cognate response regulator LiaR (EMBL entries AEP92336, CAA11744, and CAA11745, respectively) (32), which in turn regulates its own operon as well as *yvlB* (Fig. 2B) and others. In *E. faecalis* S613, the genes *yvlB* and *pspC* are likely in the same operon, and mutations in either of these genes have previously been associated with DAP resistance in enterococci (8, 10) (see Text S1 in the supplemental material). Strain TDR7 was observed to have only a single mutant allele, $yvlB^{V289fs}$, yet was DAP resistant nonetheless, suggesting that truncation of the C-terminal domain of YvlB is sufficient for resistance. Palmer et al. also observed a frameshift mutation at position Ile-390 in YvlB (EF1753) of a DAP-resistant *E. faecalis* variant (10).

As none of the adaptive mutations in LiaFSR signaling components introduced stop codons or frameshifts that would decouple the pathway response, the LiaFSR response in enterococci is likely activated by antibiotics that induce cell wall stress, as observed in *B. subtilis*, *Streptococcus mutans*, and the comparable VraTSR (vancomycin resistance-associated sensor/regulator) in *Staphylococcus aureus* (32, 35). The prevalence of mutations in *liaFSR* during DAP adaptation suggests that alteration of this signaling pathway is a general and effective response to membrane insult (7, 8, 10). Following the rise of successful adaptation through the LiaFSR pathway, nearly half of the polymorphic population then acquired mutations to *cls* (Fig. 2A).

Alterations of CL synthase activity are linked to changes in the LiaFSR pathway. Mutations to *cls* were among the most common within the population, suggesting an important role for changes to Cls activity in response to DAP. A link between Cls activity and DAP adaptation is supported by the observations that Cls catalyzes the formation of cardiolipin (CL) from two molecules of PG and that DAP activity is dependent on the presence of phosphatidylglycerol (PG) and calcium (34). Clinical isolates *E. faecalis* R712 and *E. faecium* R446 both have mutations to *cls* and a decrease in membrane PG content, as well as distinctive changes to the cell envelope following DAP exposure (36, 37). *In vitro* biochemical analysis of adaptive mutants Cls^{R218Q} and Cls^{H215R} from *E. faecium* showed that each mutation increased Cls activity (7, 38). As cls^{R218Q} was observed in *E. faecalis* strain TDR19.1, it is likely that mutations to *cls* in these populations do likewise.

Cls mutations were observed across five separate evolutionary trajectories and always followed mutations that altered LiaFSR signaling (Fig. 3A), suggesting that *cls* mutations alone were insufficient to confer clinical levels of resistance and instead may compensate for earlier changes made through the LiaFSR pathway. Indeed, replacement of a wild-type *cls* allele by a mutated one belonging to a DAP-resistant strain did not affect DAP susceptibility in *E. faecium* (36, 37). Expression of Cls^{R218Q} from a multicopy plasmid in *E. faecalis* OG1RF, however, increased the MIC_{DAP}, suggesting that in the right genomic context and with potentially higher expression levels, Cls^{R218Q} could increase resistance (10). The same adaptive mutation, Cls^{R218Q}, was also observed in DAP-resistant clinical isolates of *E. faecium* (7).

Cyclic dinucleotide and redox signaling: a new path to increased daptomycin resistance? In strains TDR4 and TDR19.2, we observed an epistatic linkage between mutant alleles $yybT^{I440S}$ and $gshF^{E354K}$, with both alleles rising simultaneously in the population prior to mutation of *cls* (Table 2; Fig. 2A). YybT homologues in both *B. subtilis* (EMBL entry CAB16088) and *S. aureus* (denoted GdpP in *S. aureus*; EMBL entry AEW64051) have cyclic di-AMP (c-di-AMP) phosphodiesterases activity, with potential roles in stress signaling and response (39–41). As a global second messenger, cyclic dinucleotide signaling has been implicated in quorum sensing, adhesion, and biofilm formation (39, 40, 42). While cyclic dinucleotide signaling has not been previously characterized in enterococci, the identification of a YybT homologue and the subsequent identification of adaptive mutations within the gene is consistent with a role for cyclic dinucleotide signaling in the stress response.

As a glutathione synthase, GshF has previously been implicated in the oxidative stress response across multiple species (43). GshF is commonly found among mammalian pathogens (44) and could have a role in mitigating DNA damage caused by general oxidative stress (43). Mutations to *yybT* and *gshF* share the common distinction of being responsive to stress-induced damage, and earlier studies have clearly shown that insertion of the DAP-Ca^{2+} complex into the membrane leads to a loss of ions (such as K^+) and functional integrity, leading to a significant increase in oxidative stress on the cell (45).

Biofilm formation is correlated to DAP resistance phenotype. Biofilm formation also increased substantially in DAP-resistant strains and appears to be associated with the resistant phenotype. After measuring growth rates of resistant strains under various concentrations of DAP, we observed a clear correlation between DAP resistance and biofilm formation among both tur-

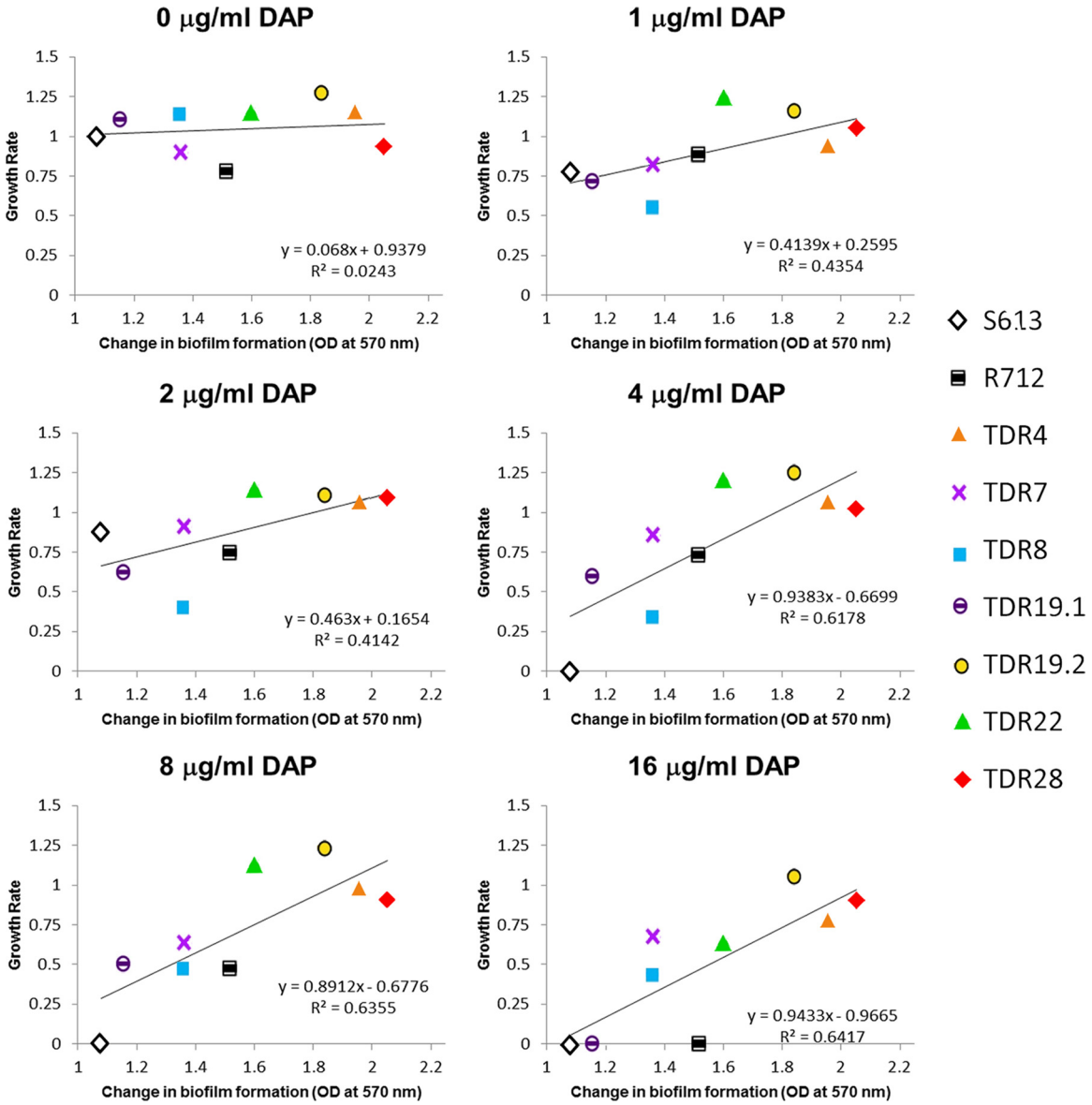

FIG 4 Changes in biofilm formation are correlated to growth rate at increasing concentrations of DAP. Correlation between data from Fig. 3B and Fig. S3 in the supplemental material is shown. Overall, strains that produce more biofilm have a higher growth rate (i.e., fitness) as the DAP concentration increases. Biofilm formation was so strong in strain TDR13 that growth rates could not be measured. Growth rates were measured over 24 h by absorbance in 96-well microtiter plates (see Fig. S1 in the supplemental material). TDR13 aggregated so severely that accurate measurement of cell numbers from optical density in 96-well plates was not possible.

bidostat-derived strains and clinically resistant strain R712 (Fig. 4). Despite this clear trend, we could not identify a single allele responsible for the phenotype but rather identified combinations of alleles whose net effect is to increase biofilm formation. Strains TDR13 and TDR28 had the most aggressive biofilm formation phenotype and were able to grow at the highest DAP concentrations. These strains included changes to uncharacterized-protein genes *drmA* and *mdpA*, respectively, in addition to *liaF* and *cls* (Table 1). TDR7 and TDR19.1, the two endpoint strains with the lowest resistance (see Fig. S1 in the supplemental material), were poor biofilm formers but still clinically resistant. Thus, increased biofilm formation itself is not required for attaining clinical levels of resistance *in vitro*, but it was clearly correlated with the majority of the successful evolutionary trajectories (Fig. 3B). It is possible that only a fraction of the total population needs to be strong biofilm formers (TDR13 and TDR28) to provide the foundation for a biofilm community that could include strains that are not strong biofilm formers themselves (TDR7 and TDR19.3), leading to a more complex and diverse biofilm community.

Clinically, biofilm formation is strongly linked to pathogenesis via adherence and resistance to phagocytosis in *E. faecalis*-mediated endocarditis and urinary tract infections (46). While *yvlB* mutations were present in weakly biofilm-forming strains TDR7 and TDR19.1, they are absent thus far in clinically identified DAP-resistant strains of *E. faecalis* (7), which is consistent with a model

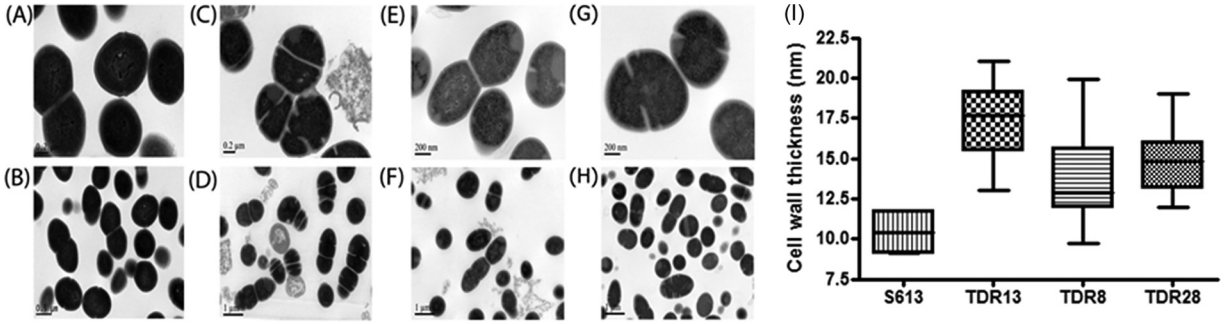

FIG 5 Transmission electron microscopy of strains TDR13, TDR8, and TDR28 shows changes to cell wall features. Relative to that in ancestral strain S613 (A and B), TEM shows abnormal septation in strain TDR13 (C and D), comparable to that in clinical strain R712 (7). In contrast, strains TDR8 (E and F) and TDR28 (G and H) show normal cell division. All TDR strains, however, showed increased cell wall thickness (I), another characteristic of strain R712.

in which biofilm formation results in a combination of resistance and pathogenicity.

Infrequent alleles appear toward the end of adaptation and may increase biofilm formation. We noted that as adaptation proceeded, mutations of increasing variety but lower overall frequency were observed. Mutations *cls*^{R218Q}, *cls*$^{insAII14-16}$, *drmA*^{L4stop}, *drmA*^{N150fs}, *mdpA*^{F185fs}, and *cls*^{S104L} were all present at less than 5% of the endpoint population and were the final mutations to arise in their respective lineages (Fig. 3A). Generally rising in frequency on the final few days of the adaptation experiment, these mutations may be epistatic with earlier changes or increase fitness very modestly. Thus, these mutations experience success only when arising in the background of much more significant changes in fitness brought about through the LiaFSR pathway (Fig. 3).

As described above, the two strains exhibiting the most aggressive biofilm formation phenotype, TDR13 and TDR28, include changes to uncharacterized-protein genes *drmA* and *mdpA*, respectively (Table 1). Bioinformatics analysis suggests that *drmA* encodes a six-pass integral membrane protein of unknown function, while *mdpA* encodes a putative ABC transporter. Mutations to *drmA* include a frameshift at position N_{150} and mutation to a stop codon at L_4, suggesting that inactivation of *drmA* is associated with increased biofilm formation. A different frameshift mutation in *drmA* was observed previously in *E. faecalis* V583 after adaptation to DAP (10) (*drmA* denoted EF1797). Likewise, the introduction of a frameshift at position 185 in the putative ABC transporter gene *mdpA* likely alters or disables protein function, leading to increased biofilm formation. Our data suggest that while mutations to *drmA* or *mdpA* may be important to the establishment of biofilms, they may have a high fitness cost that reduces their overall success within the population.

Transmission electron microscopy reveals similar morphologies for clinical and adapted strains. Previous analysis of clinical isolate *E. faecalis* R712 observed aberrant membrane structures, including septal defects and increased cell wall size, using transmission electron microscopy (7). All eight endpoint strains showed aberrant membrane structures, with septal defects and increased cell wall thickness. These changes in membrane structure varied among the eight strains, with strain TDR13 showing severe septal defects comparable to those of R712 (Fig. 5). Compared to S613 (Fig. 5A and B), representative strains TDR13 (Fig. 5C and D), TDR28 (Fig. 5E and F), and TDR8 (Fig. 5G and H) show both aberrant septal structures and multiple septal formations prior to complete cell separation. In TDR28 and TDR8, septal structures form along the cylindrical portion of the cell, with identifiable poles. The most striking changes to septation and cell division are observed in TDR13, with cells lacking a specific polarity. Several septal structures are identified within the same cell, and separation of cells is rare. The mean (± standard deviation [SD]) of cell wall thickness was determined for TDR28, TDR8, and TDR13. The cell wall thickness increased significantly in all three strains compared to S613 (Fig. 5I). The observed changes in morphology are similar to those previously observed in DAP-resistant clinical isolate R712 (7). Together these results confirm the important alterations of cell division associated with development of DAP resistance in enterococci and demonstrate that a variety of genotypes converge on a common morphological phenotype in DAP-resistant *E. faecalis*.

Contingency loci may modulate the *E. faecalis* response to stressors. Unexpectedly, we found that several mutations in *cls* and *liaF* evolved through insertions or deletions of entire codons in repeat sequences, suggesting that these sites may be contingency loci. Facilitated by such short nucleotide repeats, contingency loci are localized regions of hypermutability, which mediate "high-frequency, reversible, genotypic switching" (47). In one such case in *cls*, a direct repeat encoding $NFQNFQ_{74-79}$ in the ancestor S613 was mutated to NFQ in 42% of the final population (see Table S2 in the supplemental material), and this arose independently in the population in at least three different genetic backgrounds (assuming asexuality) (Fig. 3A), suggesting that slipping along this repeat may be quite frequent. In addition to the NFQ deletion, we also observed a duplication of AII_{14-16} in *cls* in TDR19.2 (Table 1). Like for *cls*, adaptive changes to *liaF* occurred from an insertion or deletion of an entire codon in a repeat of four Ile codons from position 177 to 182.

While short contingency loci that can slip by codons within direct repeats appear to be quite common to *E. faecalis* (see Fig. S2 in the supplemental material), they do not appear to be present in *E. faecium* (7, 8), suggesting mechanistic differences to adaptation in these two closely related species. Similarly, the adaptive mutation *gdpD*$^{\Delta I170}$ in the clinical strain R712 was also a single-codon deletion within an isoleucine repeat. Canonical contingency loci such as those in *Haemophilus influenzae* produce rapid and reversible phenotypic switching through frameshift mutations (47), but the codon slippage observed in *E. faecalis* is a highly specialized modulation of activity that may produce more nuanced changes in activity. Several genes responsible for CESR in *E. faecalis* have

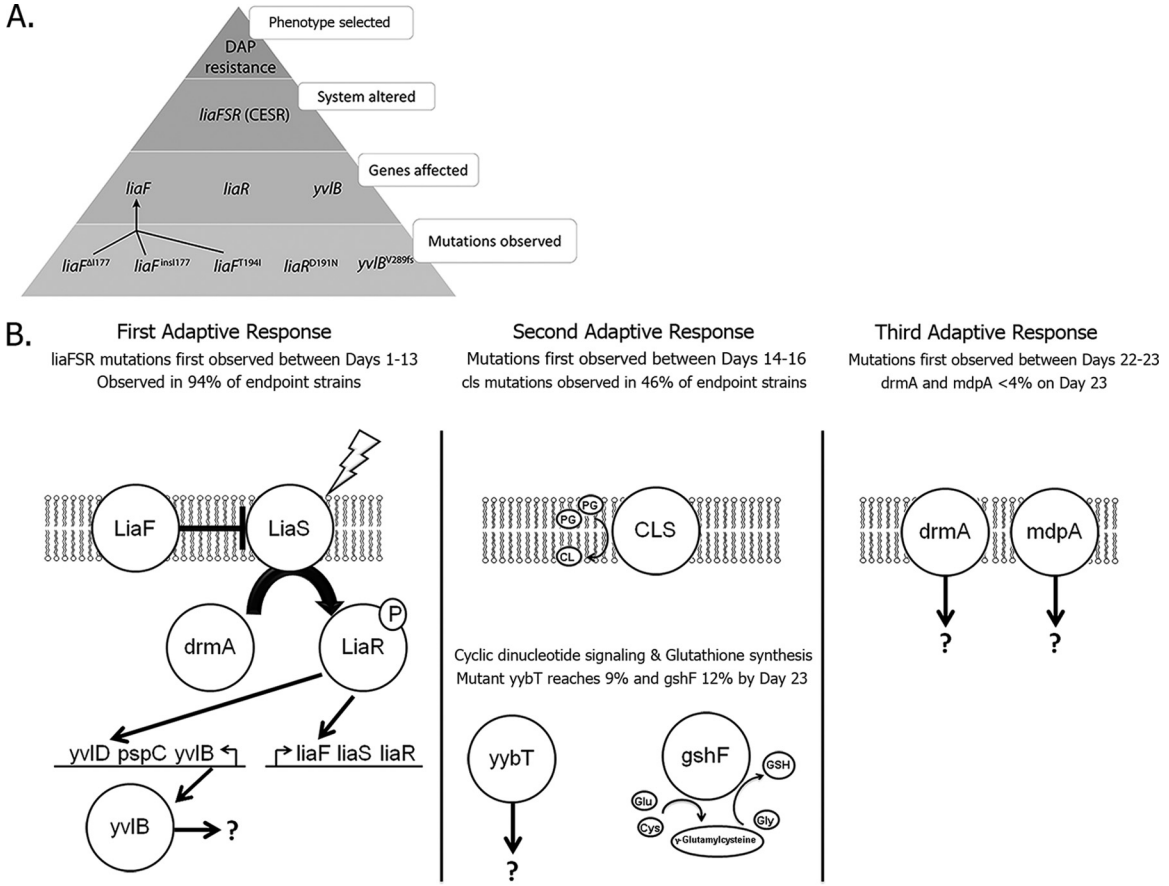

FIG 6 (A) Evolution proceeds through a conserved hierarchy of change. In biology, phenotype (e.g., DAP resistance) is the characteristic upon which natural selection is acting. Changes bringing about increased fitness are largely changes to cellular "systems" (e.g., the LiaFSR signaling network). The LiaFSR network can, in principle, be activated by any of the proteins that regulate the critical operons, such as LiaF, LiaR, or YvlB. In turn, there are numerous mutations that can increase fitness, and though they may vary in position or substitution, their conserved effect is to alter protein function to modulate LiaFSR signaling. Thus, the hierarchy of change moves from highly conserved to less conserved during adaptation. (B) Order and cellular context of the adaptive alleles. Putative localization and functions were assigned based on homologues as discussed in text and from bioinformatic analysis. Question marks denote unknown function. Proposed functions of *liaFSR* components are based on homologous proteins previously studied in *Streptococcus mutans* (35). PG, phosphatidylglycerol; CL, cardiolipin; GSH, glutathione.

these repetitive and slip-prone sequences, suggesting that these "slippery" sequences may have been selected by frequent encounters with the stressors that require facile changes to the cell envelope.

Evolution of daptomycin resistance followed a conserved hierarchy. Quantitative experimental evolution clearly identified an order and hierarchy of change that reflects the *in vivo* organizing principles of the cell as it undergoes natural selection. Figure 6 illustrates the hierarchy of organizing principles underlying adaptation to DAP. While the phenotype (DAP resistance) is the object of selection, the changes required to bring about adaptation through the LiaFSR system are less constrained and can proceed through a number of genes (*liaF*, *liaR*, and *yvlB*). In turn, the number of mutations within a specific gene that can produce the required change in protein function can be quite high, with relatively few proteins or pathways altered (Fig. 6B). Thus, while eight DAP-resistant genotypes were monitored during adaptation, they all followed the same broader evolutionary trajectory. Our results suggest that while specific mutations may vary, the pathways they affect and the phenotypes they confer are well conserved, a finding in good agreement with temperature adaptation studies by Tenaillon et al. in *E. coli* (21). Recognition of such general trends can provide an important context for the rational selection of potential drug targets and the design of new strategies for antibiotic development.

Summary and conclusions. While the ecology of the experimental evolution is much less complex than an infection within a patient, our results followed the adaptive landscapes observed *in vivo* for the development of DAP resistance during clinical infections by *E. faecalis*. By examining intermediate allelic frequencies during adaptation, quantitative experimental evolution allows the exploration of phenomena such as epistasis between adaptive alleles to reveal complex relationships within cells, and it also provides a basis for assessing the significance of smaller contributors. Cultivation of a polymorphic population also allows observation of a convergent hierarchy of adaptive mutations, as each subpopulation adapts to the same stressor. The ability to prioritize targets for further investigation is particularly important to time- and labor-intensive physicochemical and structural studies.

Our results suggest a highly constrained path to DAP resis-

tance. Out of over 3,000 possible genes, mutations were observed in only 8 alleles, representing less than 0.3% of the available sequencing space. Looking more closely, it is clear that the path to resistance clusters into two steps: changes to LiaFSR signaling followed by alterations to Cls. Even more striking is our finding that mutations in the same codons (*liaF*$^{\Delta I177}$ and *liaF*^{insI177}) were observed not only in turbidostat strains but also in clinical isolate R712. Similarly, the same mutation in *cls* was also observed in three different genetic backgrounds in the turbidostat, which in the absence of sexual recombination suggests independent and parallel evolution of this mutation. While the number of permutations open to a genome is vast, it is clear from our work and that of others that adaptation to strong selection can follow reproducible and predictable paths essential for prediction (13, 48, 49).

The mutant genes identified within the turbidostat population have been observed not only in other DAP-resistant populations of strain S613 but also in other strains and across species in *E. faecium*. Using a flask-based adaptation procedure with *E. faecalis* strain V583, Palmer et al. (10) observed mutations in *cls*, *yvlB* (denoted EF1753), and *drmA* (denoted EF1797). In *E. faecium*, Munita et al. (50) demonstrated the importance of mutations to *liaFSR* across multiple clinical isolates, while Humphries et al. (8) have identified mutations in genes *pspC* (a member of the *yvlB* operon) and *cls* in two *E. faecium* strains. In contrast to these studies however, we were able to identify not only adaptive mutations but also their order and potential epistatic relationships.

Our findings also revealed many general characteristics of adaptation in enterococci that were previously unsuspected. Among the most unexpected findings was the appearance of a robust network of subtle contingency loci that may rapidly modulate the response to stressors by deleting and inserting entire codons. In addition, two of the evolutionary trajectories identified mutations in YybT, a protein that has homology to a cyclic dinucleotide signaling protein, suggesting a potential role for cyclic dinucleotides in the stress response to antibiotics. Thus, while quantitative experimental evolution identified clear genetic and biochemical paths to adaptation, it also illuminated previously unknown features of DAP resistance.

With the rise of increasingly multidrug-resistant bacteria and a continuing decline in the number of new antibiotics, there is a clear opportunity to develop new strategies that can preclude or limit the development of resistance (1). Identifying key pathways to antibiotic resistance not only can guide development of new antibiotics but also can identify targets for the development of antievolution drugs that could be administered as adjuvants to increase antibiotic efficacy. The ability to implement this new "antievolution" strategy, however, relies on our ability to reliably anticipate mechanisms of resistance before they arrive in the community. Quantitative experimental evolution is a first step toward practical evolutionary forecasting that can generate new insights into the specific mechanisms of resistance as well as our overall understanding of evolution.

ACKNOWLEDGMENTS

We thank Siegfried Hirczy for identification of noncoding mutations in TDR strains and Michael Tschannen for assistance with FREQ-Seq.

This work was supported in part by NIH grant R01 AI080714 (Y.S.) from the National Institute of Allergy and Infectious Diseases (NIAID), grant HDTRA1010-0069 (Y.S.), NIH grant R01 AI093749 (C.A.A.) from NIAID, and a John S. Dunn Foundation Collaborative Research Award to Y.S. and C.A.A.

C.M., J.K., G.S., C.A.A., and Y.S. conceived and designed the experiments; C.M., J.K., T.T.T., and G.S. performed the experiments; C.M., J.K., T.T.T., G.S., C.A.A., and Y.S. analyzed the data; C.M., C.A.A., G.S., and Y.S. contributed reagents, material, or analysis tools; and C.M., J.K., T.T.T., C.A.A., G.S., and Y.S. wrote the paper.

REFERENCES

1. **Scott DR.** 2009. The direct medical costs of healthcare-associated infections in U.S. hospitals and the benefits of prevention. CDC, Atlanta, GA.
2. **Klevens RM, Edwards JR, Richards CL, Jr, Horan TC, Gaynes RP, Pollock DA, Cardo DM.** 2007. Estimating health care-associated infections and deaths in U.S. hospitals, 2002. Public Health Rep. **122:**160–166.
3. **Zell BL, Goldmann DA.** 2007. Healthcare-associated infection and antimicrobial resistance: moving beyond description to prevention. Infect. Control Hosp. Epidemiol. **28:**261–264.
4. **Boucher HW, Talbot GH, Bradley JS, Edwards JE, Gilbert D, Rice LB, Scheld M, Spellberg B, Bartlett J.** 2009. Bad bugs, no drugs: no ESKAPE! An update from the Infectious Diseases Society of America. Clin. Infect. Dis. **48:**1–12.
5. **Rice LB.** 2008. Federal funding for the study of antimicrobial resistance in nosocomial pathogens: no ESKAPE. J. Infect. Dis. **197:**1079–1081.
6. **Arias CA, Murray BE.** 2012. The rise of the Enterococcus: beyond vancomycin resistance. Nat. Rev. Microbiol. **10:**266–278.
7. **Arias CA, Panesso D, McGrath DM, Qin X, Mojica MF, Miller C, Diaz L, Tran TT, Rincon S, Barbu EM, Reyes J, Roh JH, Lobos E, Sodergren E, Pasqualini R, Arap W, Quinn JP, Shamoo Y, Murray BE, Weinstock GM.** 2011. Genetic basis for in vivo daptomycin resistance in enterococci. N. Engl. J. Med. **365:**892–900.
8. **Humphries RM, Kelesidis T, Tewhey R, Rose WE, Schork N, Nizet V, Sakoulas G.** 2012. Genotypic and phenotypic evaluation of the evolution of high-level daptomycin nonsusceptibility in vancomycin-resistant Enterococcus faecium. Antimicrob. Agents Chemother. **56:**6051–6053.
9. **Munoz-Price LS, Lolans K, Quinn JP.** 2005. Emergence of resistance to daptomycin during treatment of vancomycin-resistant Enterococcus faecalis infection. Clin. Infect. Dis. **41:**565–566.
10. **Palmer KL, Daniel A, Hardy C, Silverman J, Gilmore MS.** 2011. Genetic basis for daptomycin resistance in enterococci. Antimicrob. Agents Chemother. **55:**3345–3356.
11. **Munita JM, Tran TT, Diaz L, Panesso D, Reyes J, Murray BE, Arias CA.** 2013. A liaF codon deletion abolishes daptomycin bactericidal activity against vancomycin-resistant Enterococcus faecalis. Antimicrob. Agents Chemother. **57:**2831–2833.
12. **Pena MI, Davlieva M, Bennett MR, Olson JS, Shamoo Y.** 2010. Evolutionary fates within a microbial population highlight an essential role for protein folding during natural selection. Mol. Syst. Biol. **6:**387.
13. **Counago R, Chen S, Shamoo Y.** 2006. In vivo molecular evolution reveals biophysical origins of organismal fitness. Mol. Cell **22:**441–449.
14. **Elena SF, Lenski RE.** 2003. Evolution experiments with microorganisms: the dynamics and genetic bases of adaptation. Nat. Rev. Genet. **4:**457–469.
15. **Khan AI, Dinh DM, Schneider D, Lenski RE, Cooper TF.** 2011. Negative epistasis between beneficial mutations in an evolving bacterial population. Science **332:**1193–1196.
16. **Weinreich DM, Delaney NF, Depristo MA, Hartl DL.** 2006. Darwinian evolution can follow only very few mutational paths to fitter proteins. Science **312:**111–114.
17. **Chou HH, Chiu HC, Delaney NF, Segre D, Marx CJ.** 2011. Diminishing returns epistasis among beneficial mutations decelerates adaptation. Science **332:**1190–1192.
18. **Lang GI, Botstein D, Desai MM.** 2011. Genetic variation and the fate of beneficial mutations in asexual populations. Genetics **188:**647–661.
19. **Arjan JA, Visser M, Zeyl CW, Gerrish PJ, Blanchard JL, Lenski RE.** 1999. Diminishing returns from mutation supply rate in asexual populations. Science **283:**404–406.
20. **Travisano M.** 1997. Long-term experimental evolution in Escherichia coli. VI. Environmental constraints on adaptation and divergence. Genetics **146:**471–479.
21. **Tenaillon O, Rodriguez-Verdugo A, Gaut RL, McDonald P, Bennett AF, Long AD, Gaut BS.** 2012. The molecular diversity of adaptive convergence. Science **335:**457–461.
22. **Friedman L, Alder JD, Silverman JA.** 2006. Genetic changes that corre-

late with reduced susceptibility to daptomycin in Staphylococcus aureus. Antimicrob. Agents Chemother. **50:**2137–2145.
23. **Toprak E, Veres A, Michel JB, Chait R, Hartl DL, Kishony R.** 2012. Evolutionary paths to antibiotic resistance under dynamically sustained drug selection. Nat. Genet. **44:**101–105.
24. **Dykhuizen DE, Dean AM, Hartl DL.** 1987. Metabolic flux and fitness. Genetics **115:**25–31.
25. **Chubiz LM, Lee MC, Delaney NF, Marx CJ.** 2012. FREQ-Seq: a rapid, cost-effective, sequencing-based method to determine allele frequencies directly from mixed populations. PLoS One **7:**e47959. doi:10.1371/journal.pone.0047959.
26. **Wikler MA.** 2009. Methods for dilution antimicrobial susceptibility tests for bacteria that grow aerobically—approved standard, 8th ed. Clinical and Laboratory Standards Institute, Wayne, PA.
27. **Li H, Durbin R.** 2009. Fast and accurate short read alignment with Burrows-Wheeler transform. Bioinformatics **25:**1754–1760.
28. **Li H, Handsaker B, Wysoker A, Fennell T, Ruan J, Homer N, Marth G, Abecasis G, Durbin R.** 2009. The sequence alignment/map format and SAMtools. Bioinformatics **25:**2078–2079.
29. **Li H, Ruan J, Durbin R.** 2008. Mapping short DNA sequencing reads and calling variants using mapping quality scores. Genome Res. **18:**1851–1858.
30. **Walkiewicz K, Benitez Cardenas AS, Sun C, Bacorn C, Saxer G, Shamoo Y.** 2012. Small changes in enzyme function can lead to surprisingly large fitness effects during adaptive evolution of antibiotic resistance. Proc. Natl. Acad. Sci. U. S. A. **109:**21408–21413.
31. **Mohamed JA, Huang DB.** 2007. Biofilm formation by enterococci. J. Med. Microbiol. **56:**1581–1588.
32. **Wolf D, Kalamorz F, Wecke T, Juszczak A, Mader U, Homuth G, Jordan S, Kirstein J, Hoppert M, Voigt B, Hecker M, Mascher T.** 2010. In-depth profiling of the LiaR response of Bacillus subtilis. J. Bacteriol. **192:**4680–4693.
33. **Jung D, Powers JP, Straus SK, Hancock RE.** 2008. Lipid-specific binding of the calcium-dependent antibiotic daptomycin leads to changes in lipid polymorphism of model membranes. Chem. Phys. Lipids **154:**120–128.
34. **Muraih JK, Harris J, Taylor SD, Palmer M.** 2012. Characterization of daptomycin oligomerization with perylene excimer fluorescence: stoichiometric binding of phosphatidylglycerol triggers oligomer formation. Biochim. Biophys. Acta **1818:**673–678.
35. **Suntharalingam P, Senadheera MD, Mair RW, Levesque CM, Cvitkovitch DG.** 2009. The LiaFSR system regulates the cell envelope stress response in Streptococcus mutans. J. Bacteriol. **191:**2973–2984.
36. **Mishra NN, Bayer AS, Tran TT, Shamoo Y, Mileykovskaya E, Dowhan W, Guan Z, Arias CA.** 2012. Daptomycin resistance in enterococci is associated with distinct alterations of cell membrane phospholipid content. PLoS One **7:**e43958. doi:10.1371/journal.pone.0043958.
37. **Tran TT, Panesso D, Gao H, Roh JH, Munita JM, Reyes J, Diaz L, Lobos EA, Shamoo Y, Mishra NN, Bayer AS, Murray BE, Weinstock GM, Arias CA.** 2013. Whole-genome analysis of a daptomycin-susceptible Enterococcus faecium strain and its daptomycin-resistant variant arising during therapy. Antimicrob. Agents Chemother. **57:**261–268.
38. **Davlieva M, Zhang W, Arias CA, Shamoo Y.** 2013. Biochemical characterization of cardiolipin synthase mutations associated with daptomycin resistance in enterococci. Antimicrob. Agents Chemother. **57:**289–296.
39. **Christen M, Christen B, Folcher M, Schauerte A, Jenal U.** 2005. Identification and characterization of a cyclic di-GMP-specific phosphodiesterase and its allosteric control by GTP. J. Biol. Chem. **280:**30829–30837.
40. **Corrigan RM, Abbott JC, Burhenne H, Kaever V, Grundling A.** 2011. c-di-AMP is a new second messenger in Staphylococcus aureus with a role in controlling cell size and envelope stress. PLoS Pathog. **7:**e1002217. doi:10.1371/journal.ppat.1002217.
41. **Rao F, See RY, Zhang D, Toh DC, Ji Q, Liang ZX.** 2010. YybT is a signaling protein that contains a cyclic dinucleotide phosphodiesterase domain and a GGDEF domain with ATPase activity. J. Biol. Chem. **285:**473–482.
42. **Ueda A, Wood TK.** 2009. Connecting quorum sensing, c-di-GMP, pel polysaccharide, and biofilm formation in Pseudomonas aeruginosa through tyrosine phosphatase TpbA (PA3885). PLoS Pathog. **5:**e1000483.
43. **Cameron JC, Pakrasi HB.** 2011. Glutathione facilitates antibiotic resistance and photosystem I stability during exposure to gentamicin in cyanobacteria. Appl. Environ. Microbiol. **77:**3547–3550.
44. **Stout J, De Vos D, Vergauwen B, Savvides SN.** 2012. Glutathione biosynthesis in bacteria by bifunctional GshF is driven by a modular structure featuring a novel hybrid ATP-grasp fold. J. Mol. Biol. **416:**486–494.
45. **Silverman JA, Perlmutter NG, Shapiro HM.** 2003. Correlation of daptomycin bactericidal activity and membrane depolarization in Staphylococcus aureus. Antimicrob. Agents Chemother. **47:**2538–2544.
46. **Chuang-Smith ON, Wells CL, Henry-Stanley MJ, Dunny GM.** 2010. Acceleration of Enterococcus faecalis biofilm formation by aggregation substance expression in an ex vivo model of cardiac valve colonization. PLoS One **5:**e15798. doi:10.1371/journal.pone.0015798.
47. **Moxon R, Bayliss C, Hood D.** 2006. Bacterial contingency loci: the role of simple sequence DNA repeats in bacterial adaptation. Annu. Rev. Genet. **40:**307–333.
48. **Saxer G, Doebeli M, Travisano M.** 2010. The repeatability of adaptive radiation during long-term experimental evolution of Escherichia coli in a multiple nutrient environment. PLoS One **5:**e14184. doi:10.1371/journal.pone.0014184.
49. **Szendro IG, Franke J, de Visser JA, Krug J.** 2013. Predictability of evolution depends nonmonotonically on population size. Proc. Natl. Acad. Sci. U. S. A. **110:**571–576.
50. **Munita JM, Panesso D, Diaz L, Tran TT, Reyes J, Wanger A, Murray BE, Arias CA.** 2012. Correlation between mutations in liaFSR of Enterococcus faecium and MIC of daptomycin: revisiting daptomycin breakpoints. Antimicrob. Agents Chemother. **56:**4354–4359.